Biophysical Journal, Volume 99

Supporting Material

Effects of curvature and composition on α-Synuclein binding to lipid vesicles

Elizabeth R. Middleton and Elizabeth Rhoades

Protein mutagenesis
Labeling and pathological mutants were generated using a protocol based on the QuickChange mutagenesis kit (Stratagene, La Jolla, CA). It has been reported that bacterial expression of the human αS sequence results in 20% misincorporation of cysteine at position 136 instead of tyrosine (1). Replacement of TAC at codon 136 with TAT eliminates this issue, and we utilized this conservative mutation for all αS variants in this study. The native sequence of αS does not contain any cysteines; the introduction of a cysteine at residue 130 (E130C; Fig. 1) was made for site-specific labeling with maleimide-reactive Alexa 488 fluorophore (Invitrogen, Carlsbad, CA)

Protein labeling and characterization
For labeling, αS was incubated with a 3x molar ratio of fluorophore and a 10x molar ratio of TCEP for 30 minutes at room temperature. Unreacted dye was removed using two stacked 5 mL GE Hi-Trap desalting columns (GE Healthcare Life Sciences, Pittsburgh, PA), followed by separation of unlabeled αS by passage over 5 mL thiopropyl sepharose 6B column material (GE Healthcare Life Sciences). UV-Vis absorbance at 495 nm was used to quantify the Alexa 488 concentration, but was insufficiently sensitive for determination of αS concentration due to the large absorbance of Alexa 488 (ε=7800 $M^{-1}cm^{-1}$) and the lower absorbance of αS (ε=5120 $M^{-1}cm^{-1}$) at 280 nm. A Bio-Rad DC Protein Assay was used to quantify protein concentration and the labeling efficiency was calculated using these values (Bio-Rad, Hercules, CA). The labeling efficiency ranged from 80-100%.

It has been shown previously that labeling with Alexa488 at an S9C mutation does not significantly perturb binding (2). It is expected that labeling at E130C, in the C-terminal 40 residues which do not participate in binding, will also have a minimal effect on binding. The diffusion time of αS in the absence of vesicles is invariant to concentration (up to μM αS), thus we see no evidence of oligomerization or aggregation of αS at the concentrations (100 nM) and timescales (<20 minutes) used in our experiments

Chamber passivation
Passivation of chambered coverglasses was achieved by plasma treatment followed by incubation with polylysine-conjugated polyethylene glycol (PEG-PLL) prepared from a modified Pierce PEGylation protocol (Pierce, Rockford, IL). Chambers were incubated overnight with PEG-PLL solution, rinsed thoroughly with Millipore water, and stored in water before use for measurements.

Instrumentation
FCS measurements were made on a lab-built instrument based around an inverted microscope using an Olympus IX71 microscope. A continuous emission 488 nm DPSS 50 mW laser (Coherent, Santa Clara, CA) was set to 5-20 mW output power and further adjusted with neutral density filters to 5 μW power just prior to entering the microscope. Fluorescence was collected through the objective and separated from the excitation laser using a Z488rdc long pass dichroic and an HQ600/200m bandpass filter (Chroma, Bellows Falls, VT). Fluorescence was focused onto the aperture of a 50 μm optical fiber coupled to an avalanche photodiode (Perkin Elmer, Waltham, MA). A digital correlator

(Flex03LQ-12, correlator.com, Bridgewater, NJ) was used to generate the autocorrelation curve.

FCS fit equation

The general form of the autocorrelation function describing multiple diffusing components with varied brightness (3) is Eq. S1.

$$G(\tau) = \frac{\sum_i Q_i^2 N_i g_i}{\left(\sum_i Q_i N_i\right)^2} \qquad \text{(Equation S1)}$$

For a two component system this equation becomes:

$$G(\tau) = \frac{Q_1^2 N_1 g_1 + Q_2^2 N_2 g_2}{\left(Q_1 N_1 + Q_2 N_2\right)^2} \qquad \text{(Equation S2)}$$

Component 1 is defined as free protein and component 2 is defined as a freely diffusing vesicle bound to a number of proteins. Q_1 and Q_2 describe the brightness of the multiple components relative to component 1 (free protein, in our case), so Q_1 is equal to 1 and Q_2 is simply referred to as Q, representing the brightness of the vesicles with αS bound.

$$G(\tau) = \frac{N_1 g_1 + Q^2 N_2 g_2}{\left(N_1 + Q_2 N_2\right)^2} \qquad \text{(Equation S3)}$$

The denominator in Eq. S3 now describes the total number of proteins squared, where N_1 is the number of free proteins and Q_2N_2 is the number of proteins bound to vesicles. This total number will be referred to as N. We further define the fraction of free protein, F, as N_1/N, and the fraction of bound protein, 1-F, as QN_2/N. Substituting these into Eq. S3 and simplifying the expression gives:

$$G(\tau) = \frac{F * g_1}{N} * \frac{(1-F) * Q * g_2}{N} \qquad \text{(Equation S4)}$$

Writing out the explicit autocorrelation functions for g_1 and g_2 gives the final equation used for fitting binding data to find F, N and Q.

$$G(\tau) = \frac{1}{N}\left(F * \frac{1}{1+\frac{\tau}{\tau_{\alpha S}}} * \left(\frac{1}{1+\frac{s^2\tau}{\tau_{\alpha S}}}\right)^{1/2} + Q * (1-F) * \frac{1}{1+\frac{\tau}{\tau_{vesicle}}} * \left(\frac{1}{1+\frac{s^2\tau}{\tau_{vesicle}}}\right)^{1/2} \right) \qquad \text{(Equation S5)}$$

About Q

Q is expected to be a distribution of brightnesses that reflects variability in the number of proteins bound to each individual vesicle sample, rather than a single value. We performed simulations where autocorrelation curves were generated using various brightness distributions to describe the vesicle component. Noise was added to these

curves using the variance from actual measurements and then the curves were refit using Eq. S5. For each brightness distribution, the value of Q returned by the fit was the population weighted average of all the Q values that were entered into the simulation data. These simulations suggest that a heterogeneous distribution of proteins bound (i.e. the fact the each vesicle does not have the same number of proteins bound) is not problematic for fitting our data.

Our data suggest that binding vesicles does not change the quantum yield of the Alexa 488-labeled αS. This implies that Q is also a direct measurement of the average number of proteins bound per vesicle. However, we found that Q values were often difficult to interpret. This difficulty was also pointed out by McLaughlin and Rädler and coworkers in their study of the MARCKS peptide binding to lipid vesicles by FCS (4). As in this study, we relied on the first term in Eq. S5, which has no explicit dependence upon Q, for extracting F, the fraction of unbound protein, and then calculated the fraction of bound protein from this value.

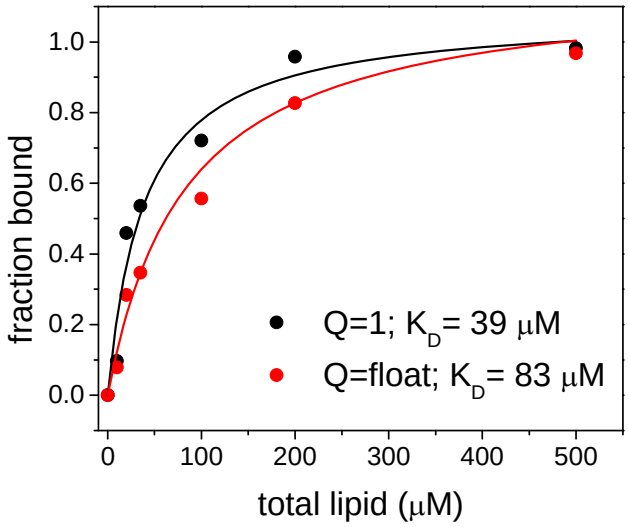

Figure S1. Effect of Q on measuring K_D. We have fit the same set of data either allowing Q to float (red) or setting Q=1. As illustrated in the plot above, we find that when Q is allowed to float, the K_D is generally shifted to the right (lower affinity) relative to when it is set equal to 1. Fitting of the curves yields approximately a factor of 2 difference in the K_D values. This shift is seen consistently throughout the data, so that we expect all of the calculated values should be similarly affected.

Calculating accessible lipid concentration and lipid volume

The concentration of accessible lipids was used for plotting binding curves and the fraction of accessible lipids was used in partition coefficient calculations. The fraction of lipid in the outer membrane is the surface area of the outer monolayer sphere ($4\pi R_{out}^2$) divided by the total inner and outer surface areas ($4\pi(R_{in}^2 + R_{out}^2)$), where R_{in} and R_{out} are the radii of the inner and outer leaflets of the membrane respectively. R_{in} and R_{out} differ

by the thickness of the membrane, d. The ratio becomes $R_{out}^2/((R_{out}-d)^2+R_{out}^2)$, where R_{out} is the radius determined by dynamic light scattering, and thicknesses (d) are listed in Table S1. The outer membrane was found to contain 55% of the lipids in a fluid phase vesicle with 93 nm diameter. The accessible lipid concentration is the fraction of lipids on the outer membrane times the total lipid concentration. For partition coefficient calculations, the volumes of one lipid molecule are listed in Table S1. The volume of lipid available for partitioning was calculated from the surface accessible lipid concentration using the volume of one lipid. Only the volume of the outer lipid bilayer was considered since we found no evidence that αS can access the inner lipid bilayer (5).

Table S1

Lipid	**Bilayer Thickness (Å)**	**Volume per lipid (Å^3)**
POPS	44.5 (6)	1256 (7)
POPC	40.5 (6)	1256 (7)
POPG	44.5 (6)	1256 (7)
POPA	45.6 (6)	1256 (7)
DPPG	56 (8)	1098 (8)
DPPC	48.2 (9)	1148 (10)

Determining $\tau_{\alpha S}$ and $\tau_{vesicle}$

$\tau_{\alpha S}$ was obtained from an αS-only solution, whereas the highest lipid concentration of vesicle titration was used for $\tau_{vesicle}$, as very little free protein is expected at that point. These data were fit to Eq. S6 for one-component diffusion to obtain $\tau_{\alpha S}$ and $\tau_{vesicle}$.

$$G(\tau)=\frac{1}{N}*\frac{1}{1+\frac{\tau}{\tau_D}}*\left(\frac{1}{1+\frac{s^2\tau}{\tau_D}}\right)^{1/2} \qquad \text{(Equation S6)}$$

As shown below, the good correlation between vesicle radius measured by DLS and the diffusion times of the vesicles measured as described above indicates that we are able to determine the vesicle diffusion time accurately.

Dynamic light scattering

Dynamic light scattering (DLS) was used to determine the diameter of the extruded or sonicated vesicles. Measurements were made on a DynaPro Titan DLS system (Wyatt Technology, Santa Barbara, CA) in the Keck Foundation Biotechnology Resource Laboratory at Yale University. The vesicle samples were 100 μM total lipid concentration and each data set consisted of an average of 30 measurements of 10 seconds each. Data were weighted for intensity and the standard deviation was calculated by multiplying the measured diameter by the percent polydispersion of the fit.

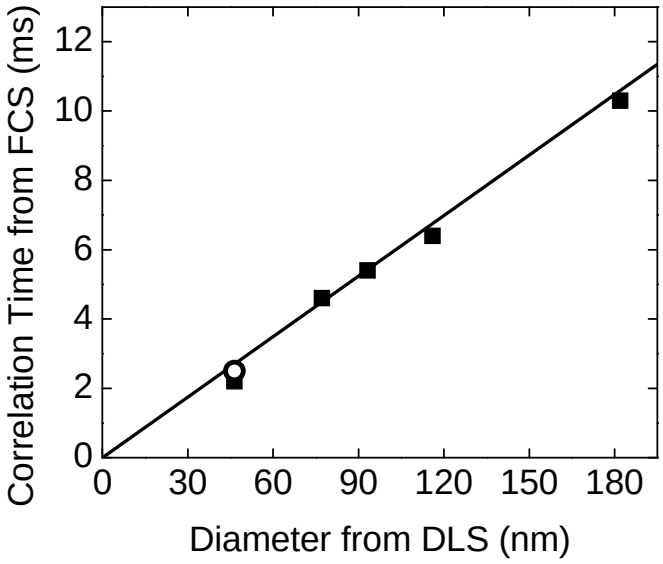

Figure S2. Characterization of vesicles by DLS and FCS. Vesicle correlation times measured by FCS (from Eq. 2 in the *Materials and Methods*) are linear with vesicle diameters measured by DLS (*black squares*). Conversion of the FCS diffusion times to particle diameters using fluorescent bead standards (Polysciences, Warrington, PA) (*black line*), showed very good agreement between vesicle size determination by FCS and DLS. This finding also suggests that although the vesicle population is polydisperse, the population of vesicles measured by αS binding is representative of the true population. If αS bound preferentially to some subset of the vesicles based on their size, we would expect to see a deviation in the relationship between DLS-measured size (which is independent of fluorescence) and FCS diffusion times and the calibration curve measured by fluorescent beads. The only exception to this observation was seen with SUVs, where we found the diffusion time of the vesicles appeared to decrease slightly as the amount of lipid was increased relative to the protein concentration. We attributed this to preferential binding to smaller vesicles within the SUV population which becomes apparent when there is excess lipid available (11). When the SUV correlation time is measured using rhodamine-labeled vesicles, as opposed to binding of αS, there is a slight improvement in the relationship between DLS and FCS (*open circle*).

Vesicle disruption

The addition of unlabeled αS to 1:1 POPS/POPC vesicles (labeled with Nile Red for observation) to a concentration equivalent to ~1:6 protein/lipid resulted in no observable changes in the autocorrelation curve that would indicate aggregation (Fig. S3) (12). DLS measurements confirm this observation (data not shown). In addition, when αS was added to vesicles encapsulating the dye/quencher pair ANTS/DPX to a protein/lipid ratio of ~1:7, there was no evidence of dye leakage which would indicate significant permeabilization or disruption of the lipid bilayer (data not shown). Both aggregation and

membrane disruption have been found previously to depend strongly on specific lipid compositions, protein/lipid ratios, and vesicle curvatures. In addition, oligomers or fibrils are more adept at causing these perturbations (13, 14). Monomeric αS used at low concentrations in our experiments reduces the probability of perturbing the membrane and is consistent with previous results showing the absence of leakage (2).

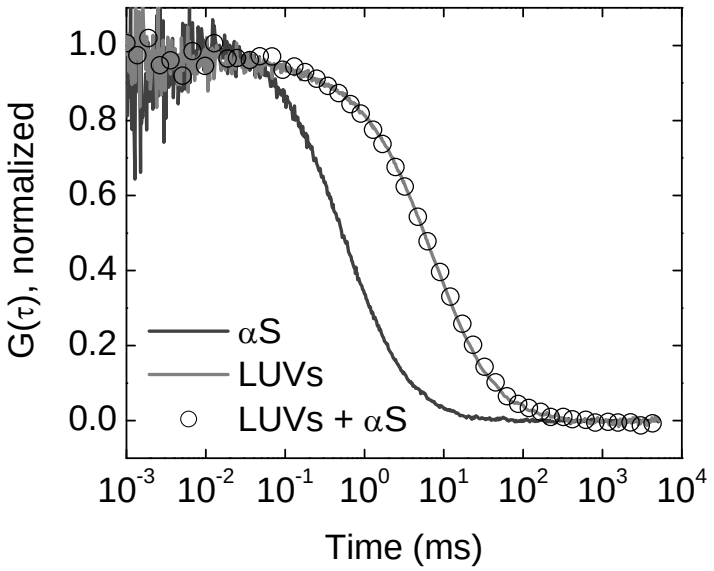

Figure S3. Binding of αS to vesicles. Normalized autocorrelation curves for αS (*dark gray*) and vesicles labeled with Nile red in the absence (*light gray*) and presence (*open circles*) of unlabeled αS at ~1:6 protein/accessible lipid. These curves show that αS does not cause vesicle aggregation or otherwise severely alter vesicle diffusion.

1. Masuda, M., N. Dohmae, T. Nonaka, T. Oikawa, S.-i. Hisanaga, M. Goedert, and M. Hasegawa. 2006. Cysteine misincorporation in bacterially expressed human α-synuclein. *FEBS Lett.* 580:1775-1779.
2. Rhoades, E., T. F. Ramlall, W. W. Webb, and D. Eliezer. 2006. Quantification of α-synuclein binding to lipid vesicles using fluorescence correlation spectroscopy. *Biophys. J.* 90:4692-4700.
3. Thompson, N. L. 1991. Fluorescence correlation spectroscopy. In Topics in Fluorescence Microscopy. J. Lakowicz, editor. Plenum Press, New York. 337-378.
4. Rusu, L., A. Gambhir, S. McLaughlin, and J. Radler. 2004. Fluorescence correlation spectroscopy studies of peptide and protein binding to phospholipid vesicles. *Biophys. J.* 87:1044-1053.
5. Perlmutter, J. D., A. R. Braun, and J. N. Sachs. 2009. Curvature dynamics of alpha-synuclein familial Parkinson disease mutants: molecular simulations of the micelle- and bilayer-bound forms. *J. Biol. Chem.* 284:7177-7189.

6. Dickey, A., and R. Faller. 2008. Examining the Contributions of Lipid Shape and Headgroup Charge on Bilayer Behavior. *Biophys. J.* 95:2636-2646.
7. Kucerka, N., S. Tristram-Nagle, and J. F. Nagle. 2006. Structure of Fully Hydrated Fluid Phase Lipid Bilayers with Monounstaturated Chains. 208:193-202.
8. Pabst, G., S. Danner, S. Karmakar, G. Deutsch, and V. A. Raghunathan. 2007. On the Propensity of Phosphatidylglycerols to Form Interdigitated Phases. *Biophys. J.* 93:513-525.
9. Giyoong, T., Y. Hosung, S. Kwanwoo, K. S. Sushil, and T. Naoya. 2008. X-ray reflectivity study of a transcription-activating factor-derived peptide penetration into the model phospholipid monolayers. 14:461-468.
10. Sun, W. J., R. M. Suter, M. A. Knewtson, C. R. Worthington, S. Tristramnagle, R. Zhang, and J. F. Nagle. 1994. Order and Disorder in Fully Hydrated Unoriented Bilayers of Gel Phase Dipalmitoylphosphatidylcholine. *Phys Rev E.* 49:4665-4676.
11. Pu, M. M., X. M. Fang, A. G. Redfield, A. Gershenson, and M. F. Roberts. 2009. Correlation of Vesicle Binding and Phospholipid Dynamics with Phospholipase C Activity: Instights into Phosphatidylcholine Activation and Surface Dilution Inhibition *J. Biol. Chem.* 284:16099-16107.
12. Elbaum-Garfinkle, S., T. Ramlall, and E. Rhoades. 2010. The role of the lipid bilayer in tau aggregation. *Biophys. J.* 98:2722-2730.
13. Giannakis, E., J. Pacífico, D. P. Smith, L. W. Hung, C. L. Masters, R. Cappai, J. D. Wade, and K. J. Barnham. 2008. Dimeric structures of α-synuclein bind preferentially to lipid membranes. *Biochim. Biophys. Acta - Biomemb.* 1778:1112-1119.
14. Volles, M. J., and P. T. Lansbury. 2002. Vesicle permeabilization by protofibrillar alpha-synuclein is sensitive to Parkinson's disease-linked mutations and occurs by a pore-like mechanism. *Biochemistry.* 41:4595-4602.